54th AIAA/ASME/ASCE/AHS/ASC Structures, Structural Dynamics, and Materials Conference
April 8-11, 2013, Boston, Massachusetts

AIAA 2013-1474

On Multiscale Modeling: Preserving Energy Dissipation across the Scales with Consistent Handshaking Methods

Evan J. Pineda [*] and Brett A. Bednarcyk [†] and Steven M. Arnold[‡]
NASA Glenn Research Center, Cleveland, OH, 44135, U.S.A.

Anthony M. Waas [§]
University of Michigan, Ann Arbor, MI, 48109, U.S.A.

Downloaded by Evan Pineda on April 26, 2013 | http://arc.aiaa.org | DOI: 10.2514/6.2013-1474

A mesh objective crack band model was implemented within the generalized method of cells micromechanics theory. This model was linked to a macroscale finite element model to predict post-peak strain softening in composite materials. Although a mesh objective theory was implemented at the microscale, it does not preclude pathological mesh dependence at the macroscale. To ensure mesh objectivity at both scales, the energy density and the energy release rate must be preserved identically across the two scales. This requires a consistent characteristic length or localization limiter. The effects of scaling (or not scaling) the dimensions of the microscale repeating unit cell (RUC), according to the macroscale element size, in a multiscale analysis was investigated using two examples. Additionally, the ramifications of the macroscale element shape, compared to the RUC, was studied.

I. Introduction

An advantage composites possess over most monolithics as a structural engineering material is that, in addition to the physical properties of the constituents, the subscale geometry (architecture) of the constituents contribute to the apparent response of the composite, yielding a material which exhibits behavior that surpasses the sum of its constituents. Often, these details are smeared into a homogenized model for convenience, and ad-hoc assumptions are used to include the effects of the composite micro-architecture, in computational analysis methods. These assumptions work well to predict the elastic behavior of composite materials. However, to incorporate the non-linear effects of damage and failure, increasingly complicated continuum damage theories and failure criteria must be developed, such as those included in numerous review papers and books.[1–7] Many, but not all, of these theories incorporate various non-physical parameters that must be calibrated in order to capture the appropriate failure modes in the composite.

The deficiencies of homogenized models become more apparent when strain localization leading to softening damage occurs in the material. Once localization occurs, the characteristic length of the material transitions from a length on the order of hundreds to thousands of repeating unit cells (RUCs) to that on the order of a representative volume element (RVE) composed of enough microstructural elements (grains, inclusions, etc.), such that the RVE behavior is typical of the bulk composite (with an embedded localization), on average. Typically, an RUC does not have a physical length associated with it, but an RVE must have a physical length associated with it, and the RVE must contain a large enough volume that it captures the essence of the microstructure from a physical standpoint. Ref. 8, 9 have studied the effect of the RVE size on deformation. However, when there is localization, the adequate RVE size will be different. Thus, the progression of strain localization is affected directly by the microscale fields in the RVE. For example,

---

[*] Aerospace Research Engineer, Mechanics and Life Predictions Branch, 21000 Brookpark Rd., AIAA member.

[†] Aerospace Research Engineer, Mechanics and Life Predictions Branch, 21000 Brookpark Rd., AIAA senior member.

[‡] Branch Chief, Mechanics and Life Predictions Branch, 21000 Brookpark Rd., AIAA senior member.

[§] Felix Pawlowski Collegiate Professor, Department of Aerospace Engineering, AIAA fellow.

This material is declared a work of the U.S. Government and is not subject to copyright protection in the United States.

Downloaded by Evan Pineda on April 26, 2013 | http://arc.aiaa.org | DOI: 10.2514/6.2013-1474

if the RVE is in a compressive load environment, fiber kink-banding (localization) within the RVE leads to a post-peak softening response influenced by the size of the RVE as shown in studies reported by.[10] If the RVE is too small, a constraining effect leads to a kink band that shows a lower peak strength when compared to the asymptotic value of peak strength associated with a larger RVE that leads to the formation of an unconstrained and "free" kink band.

Multiscale modeling is a popular technique for incorporating microscale effects into a structural scale model. With these methods, micromechanics models are linked to structural models and localization details, at the microscale, are captured directly during down-scaling, while homogenization is employed for up-scaling, to communicate the effects of localization by smearing over the subscale model. The linking of scales can be achieved in a hierarchical, concurrent, or synergistic sense.[11] With hierarchical multiscale approaches, micromechanics or subscale simulations are preformed *a priori*, and the results obtained from those simulations are utilized in subsequent macroscale, or structural level, models. With concurrent multiscale modeling, both the micro and macro scales operate simultaneously in time and space. Finally, synergistic multiscale models operate concurrently in time and hierarchically in both spatial scales (up-scaling and down-scaling), or vice versa.

The micromechanics models employed can be either analytical, semi-analytical, or fully numerical. Typically, analytical methods utilize mean field theories which are very efficient but only offer a single set of fields for each constituent.[12,13] Fully numerical methods use the finite element method (FEM) or the boundary element method to model the microscale.[14–16] These methods can be computationally expensive; however, numerous authors have developed techniques to simplify the subscale FEM problem, yielding significant speed-up, for instance, we cite,.[7,16–22] Semi-analytical methods offer the best balance between computational efficiency and solution fidelity.[23–29] There exist a plethora of multiscale techniques for fiber-reinforced composites in the literature, some of which, relevant to the present paper, have been reported in Ref. 11, 29–35.

Physically, a continuum material must posses a positive-definite tangent stiffness tensor, and, in fact, at a small enough scale, the material tangent stiffness tensor always remains positive-definite in order to satisfy the necessity of having a real, local speed of sound.[36] However for practical purposes, engineers must model structures at scales much larger than the characteristic flaws in the material. The homogenized (over a representative volume whose characteristic length is larger than the typical flaw size) continuum representation of a material containing the nucleation and propagation of discontinuities, such as cracks or voids, will exhibit post-peak strain softening in the macroscopic stress-strain response. Although micromechanics and multiscale methods can be utilized to introduce details of the composite microstructure into structural analyses, erroneous numerical failure predictions can be obtained when post-peak strain softening is exhibited in the material, regardless of the scale. Loss of positive-definiteness of the tangent stiffness tensor leads to a material instability, which manifests as a localization of damage into the smallest length scale in the continuum problem.[36] Since the post-peak stress-strain relationship prescribes the energy density dissipated during the failure process, the total amount of energy dissipated is proportional to the size of the localization element, and in the limit as the element size is decreased, zero energy is required to fail the structure.[37,38] Thus, the computational results will become pathologically dependent on the mesh size.

A simple way to overcome this deficiency is to judiciously scale the post-peak softening slope by the characteristic element length such that the total energy release rate in the post-peak regime, after reaching a state of zero stress, is equal to the critical energy release rate, or fracture toughness, of the material (a fixed, experimentally obtained material parameter). This approach, known as the crack band or smeared crack approach, has been used by many authors to model strain localization due to failure within an FEM framework in a mesh objective manner.[36,39–44] Recently, the authors, Ref. 45,46, have implemented the crack band model within the generalized method of cells (GMC)[23] and high-fidelity generalized method of cells (HFGMC)[25] micromechanics theories and the predictions were verified against analogous FEM models. Non-local, or gradient-based theories have also been shown to prevent strain localization, eliminating dependence of the numerical solution on the size of the elements, as discussed in,.[47–49] However, the latter techniques require higher-order numerical interpolations and can be challenging to implement.

Once a mesh objective theory has been implemented in a single scale analysis, the energy dissipation is preserved regardless of the size of the mesh, at that scale. However in a multiscale analysis, careful attention must be paid to how energy is being preserved and transferred across the various length scales. Ref. 50 commented that many multiscale models fail to define an appropriate localization limiter at the macroscale or fail to deliver any localization limiter to the macroscale from the microscale. If this is not

This material is declared a work of the U.S. Government and is not subject to copyright protection in the United States.

achieved energy dissipation is not necessarily preserved across the scales. However, if the appropriate theories are in employed at the correct scales and a consistent "handshaking" methodology is used that yields an appropriate localization limiter at the macroscale, then both the energy density and energy release rate will be preserved across the scales.

The objective of the present paper, therefore, is to describe a method, using a two-scale analysis, that is energy preserving (in the sense of dissipation in the post-peak regime) at both scales with the requirement of consistent characteristic length relationships across the two scales. The method described is general, and its extension to multiple-scale (more than two length scales) analysis will become apparent. In Section IV, the effects of judiciously scaling the microscale RUC size to correspond to the macroscale element size are presented for two different multiscale example problems.

II. Discretization Objective Progressive Failure Modeling at the Microscale

The objective of multiscale modeling is to incorporate the influence of the material microstructure, at a suitable length scale, on the overall macroscopic response of the composite structure. To achieve this feasibly, an efficient microscale model is required. However, some fidelity at the microscale must be maintained if multiscale modeling is to realize any benefit. GMC offers an excellent balance between efficiency and fidelity, and is ideal for multiscale modeling. Since the method is semi-analytical, it offers computational speed that is superior to FEM based models (orders of magnitude faster). Additionally, GMC can be used to calculate local field distributions (essential for nonlinear problems involving inelasticity and damage), as opposed to mean field theories, which only offer a single field value (some chosen measure of the average) per constituent.

Along with an appropriate microscale theory, physics-based constitutive laws (for the constituents in the composite) must be implemented for predictive capability. GMC admits a variety of linear and nonlinear constitutive laws, as well as any number of constituents. If the constitutive response of each constituent exhibits positive-definite behavior, then any suitable theory can be readily implemented within GMC. However, if the constitutive law exhibits post-peak strain softening behavior (i.e., a negative tangent stiffness), then an appropriate formulation must be used to ensure objectivity with respect to refinement of the discretization used to represent the microstructure.

One way to alleviate dependence on the level of discretization is to scale the energy density dissipated during the failure process, such that the energy release rate is preserved, independent of the size of the discretization element. One such model, the crack band theory,[39] was implemented within the GMC and HFGMC micromechanics theories to alleviate dependence of the failure solution on the size of the subcells used to discretize the RUC, as described earlier in Ref. 45,46. This implementation was utilized in this work to eliminate pathological dependence of the dissipated energy on the size of the subcells at the microscale.

II.A. Implementation of the Crack Band Theory within GMC

II.A.1. Physical behavior of crack band

The crack band model is intended to capture the behavior of a region of a material wherein numerous microcracks have initiated, and they eventually coalesce to form a larger crack. Figure 1 displays a crack band of width w_c embedded in a continuum. The domain of the crack band is denoted as Ω' and the remaining continuum as Ω. The crack band is oriented within the continuum such that, for a given point within the crack band, the unit vector normal to the crack band is $\boldsymbol{n}$.

The total energy dissipated during the failure process is smeared over Ω', and the size w_c of Ω' is a material property (characteristic length) directly related to the material fracture toughness.[39]

$$w_c = \frac{2\mathcal{G}_C}{\sigma_C^2}\left(\frac{1}{E} - \frac{1}{E_T}\right)^{-1} \tag{1}$$

where σ_C is the critical stress for initiation of the post-peak regime in the 1D material stress-strain law, and E_T is the negative tangent slope in that regime. The fracture toughness $\mathcal{G}_C$, or critical strain energy release rate, of the material is given by the area under the 1D traction-separation law that governs the cohesive response of the separation of crack faces as a crack propagates in the material. The energy density dissipated during failure W_F is related to the material fracture toughness through the characteristic length in the material.

$$\mathcal{G}_C = w_c W_F \tag{2}$$

Downloaded by Evan Pineda on April 26, 2013 | http://arc.aiaa.org | DOI: 10.2514/6.2013-1474

This material is declared a work of the U.S. Government and is not subject to copyright protection in the United States.

II.A.2. Formulation of crack band model

Figure 2 shows a discretization of the continuum displayed in Figure 1. A magnified view of the crack band embedded in a single GMC subvolume (i.e., subcell) is also displayed in Figure 2. Since all of the energy dissipated in the crack band is smeared over the subcell volume, the subcell must be large enough to contain the crack band of width w_C. Note that Figure 2 shows a 2D geometry for illustrative purposes, but the crack bands can also evolve in a general 3D setting.

In GMC, a doubly-periodic RUC is represented with N_β x N_γ subcells. A GMC representation of a unidirectional, fiber-reinforced composite containing square-packed fibers is shown in Figure 3. Although a 2D representation is shown, the calculated, local fields in the RUC are fully 3D, but there is no variation in the fields along the x_1-direction. Subcells in the RUC are identified by the indices β (in the x_2-direction) and γ (in the x_3-direction), and the RUC dimensions are given by H and L.

The orientation of the crack band in subcell $\beta\gamma$ is given by the vector $\boldsymbol{n_1^{(\beta\gamma)}}$ (see Figure 2) and is determined from the local principal stress state $(\bar{\sigma}_1^{(\beta\gamma)}, \bar{\sigma}_2^{(\beta\gamma)}, \bar{\sigma}_3^{(\beta\gamma)})$. In a monolithic material, it is postulated that cracks orient such that the crack tips are always subjected to pure mode I (opening mode) conditions unless there are constraints that restrict the crack orientation. These constraints can be the interface between two constituents, the interface between two adjacent plies, or a compressive loading state. Utilizing micromechanics, the constituents within the composite material are modeled discretely as separate, monolithic materials. Thus, in the pure matrix, there is nothing to constrain the crack band, and it can be assumed the crack band orients perpendicular to $\bar{\sigma}_1^{(\beta\gamma)}$, the principal stress with the largest magnitude, $|\bar{\sigma}_1^{(\beta\gamma)}| > |\bar{\sigma}_2^{(\beta\gamma)}| > |\bar{\sigma}_3^{(\beta\gamma)}|$, if $\bar{\sigma}_1^{(\beta\gamma)} \geq 0$ (tensile). Under these conditions, a crack oriented as such, is subjected to locally pure mode I loading, which is the most energetically favorable state. Although, the resulting global behavior may appear to be mixed mode because of the influence of the fibers on the local stress state driving the matrix crack band path. Crack band initiation is determined using a very simple, but physically-based criterion.[3,4]

$$\frac{\bar{\sigma}_1^{(\beta\gamma)}}{\sigma_C^{(\beta\gamma)}} = 1, \qquad \bar{\sigma}_1^{(\beta\gamma)} \geq 0 \tag{3}$$

where $\sigma_C^{(\beta\gamma)}$ is the cohesive strength of the matrix material. Once the crack band has initiated, the crack band orientation is assumed to be fixed within a particular subcell, as time evolves. If the direction of maximum principal stress is deemed an unsuitable choice for the crack band normal, other directional measures can be readily employed to determine the crack band orientation.

Once the orientation of the crack band has been determined, the subcell compliance is rotated into the principal frame using the transformation matrix.

$$\boldsymbol{T} = [\boldsymbol{n_1^{(\beta\gamma)}} \boldsymbol{n_2^{(\beta\gamma)}} \boldsymbol{n_3^{(\beta\gamma)}}][\boldsymbol{e_1} \boldsymbol{e_2} \boldsymbol{e_3}] \tag{4}$$

where $\boldsymbol{n_1^{(\beta\gamma)}}$, $\boldsymbol{n_2^{(\beta\gamma)}}$, and $\boldsymbol{n_3^{(\beta\gamma)}}$ are the principal stress directions, and $\boldsymbol{e_1}$, $\boldsymbol{e_2}$, and $\boldsymbol{e_3}$ are the unit basis vectors. All material degradation due to crack band evolution is imposed on the rotated compliance $\boldsymbol{\bar{S}^{(\beta\gamma)}}$, the components of which are given by:

$$\bar{S}_{ijkl}^{(\beta\gamma)} = T_{pi} T_{qj} S_{pqrs}^{(\beta\gamma)} T_{kr} T_{ls} \tag{5}$$

The strain energy released during the formation of new surfaces corresponding to the growth of cracks within the crack band is assumed to be dissipated over the entire subcell volume. Therefore, the post-peak softening slope $E_{IT}^{(\beta\gamma)}$, and the strain at which the principal stress state is zero $\epsilon_F^{(\beta\gamma)}$, are calculated using the characteristic length of the subcell $l_C^{(\beta\gamma)}$ and the material fracture toughness $\mathcal{G}_{IC}^{(\beta\gamma)}$.

$$\epsilon_F^{(\beta\gamma)} = \frac{2\mathcal{G}_{IC}^{(\beta\gamma)}}{\sigma_C^{(\beta\gamma)} l_C^{(\beta\gamma)}} \tag{6}$$

$$E_{IT}^{(\beta\gamma)} = \left(\frac{1}{\bar{E}_{110}} - \frac{\epsilon_F^{(\beta\gamma)}}{\sigma_C^{(\beta\gamma)}} \right)^{-1} \tag{7}$$

where $\bar{E}_{110}$ is the undamaged, axial Young's modulus in the principal frame. The characteristic length of the subcell $l_C^{(\beta\gamma)}$ is determined as the dimension of the subcell running parallel to $\boldsymbol{n_1^{(\beta\gamma)}}$ (see Figure 2).

Downloaded by Evan Pineda on April 26, 2013 | http://arc.aiaa.org | DOI: 10.2514/6.2013-1474

This material is declared a work of the U.S. Government and is not subject to copyright protection in the United States.

It should be noted that $E_{IT}^{(\beta\gamma)}$ must be less than zero; therefore, by Equations (6) and (7), a restriction is placed on the maximum allowable subcell size.

$$l_C^{(\beta\gamma)} < \frac{2\mathcal{G}_{IC}^{(\beta\gamma)}\bar{E}_{110}}{{\sigma_C^{(\beta\gamma)}}^2} \tag{8}$$

Use of a subcell violating Equation (8) results in non-physical snap-back. If this is unavoidable, the strength of the material can be scaled to accommodate size effects, and a sudden drop in the stress to zero can be employed subsequent to failure initiation, as descried in,.[39] In addition to a maximum size restriction, the subcells must also be larger than the actual characteristic length of the material w_C.

$$w_C \leq l_C^{(\beta\gamma)} \tag{9}$$

If the subcell size is smaller than w_C, then non-local theories must be used because it is unrealistic for the failure to localize to a scale smaller than the characteristic length of the material; thus, localization to a single subcell must be prevented outright.

The local, rotated, subcell strain state $\bar{\epsilon}_i^{(\beta\gamma)}$

$$\left\{ \begin{array}{c} \bar{\epsilon}_1^{(\beta\gamma)} \\ \bar{\epsilon}_2^{(\beta\gamma)} \\ \bar{\epsilon}_3^{(\beta\gamma)} \end{array} \right\} = \left\{ \begin{array}{c} T_{1i}^{(\beta\gamma)}\bar{\epsilon}_{ij}^{(\beta\gamma)}T_{1j}^{(\beta\gamma)} \\ T_{2i}^{(\beta\gamma)}\bar{\epsilon}_{ij}^{(\beta\gamma)}T_{2j}^{(\beta\gamma)} \\ T_{3i}^{(\beta\gamma)}\bar{\epsilon}_{ij}^{(\beta\gamma)}T_{3j}^{(\beta\gamma)} \end{array} \right\} \tag{10}$$

is used to degrade the rotated compliance components. The scalar, mode I, damage factor $D_I^{(\beta\gamma)}$ is calculated using the rotated strain corresponding to $\bar{\sigma}_1^{(\beta\gamma)}$.

$$D_I^{(\beta\gamma)} = 1 + \frac{E_{IT}^{(\beta\gamma)}\left(\epsilon_C^{(\beta\gamma)} - \bar{\epsilon}_1^{(\beta\gamma)}\right)}{\bar{E}_{110}\bar{\epsilon}_1^{(\beta\gamma)}} \tag{11}$$

where $\epsilon_C^{(\beta\gamma)}$ is the value of $\bar{\epsilon}_1^{(\beta\gamma)}$ when the initiation criterion, Equation (3), is satisfied. If $D_I^{(\beta\gamma)}$ is less than zero, no damage occurs, while a maximum damage level of one corresponds to a zero stress state on the softening stress-strain curve. Also, damage healing is inadmissable.

$$\dot{D}_I^{(\beta\gamma)} \geq 0 \tag{12}$$

The components of the rotated compliance matrix are degraded with the damage factor according to:

$$\bar{\boldsymbol{S}}^{(\boldsymbol{\beta\gamma})} = \begin{bmatrix} \dfrac{\bar{S}_{1111}^{0^{(\beta\gamma)}}}{\left(1 - D_I^{(\beta\gamma)}\right)} & \bar{S}_{1122}^{(\beta\gamma)} & \bar{S}_{1133}^{(\beta\gamma)} & 0 & 0 & 0 \\ \bar{S}_{1122}^{(\beta\gamma)} & \bar{S}_{2222}^{(\beta\gamma)} & \bar{S}_{2233}^{(\beta\gamma)} & 0 & 0 & 0 \\ \bar{S}_{1133}^{(\beta\gamma)} & \bar{S}_{2233}^{(\beta\gamma)} & \bar{S}_{3333}^{(\beta\gamma)} & 0 & 0 & 0 \\ 0 & 0 & 0 & \bar{S}_{2323}^{(\beta\gamma)} & 0 & 0 \\ 0 & 0 & 0 & 0 & \dfrac{\bar{S}_{1313}^{0^{(\beta\gamma)}}}{\left(1 - D_I^{(\beta\gamma)}\right)} & 0 \\ 0 & 0 & 0 & 0 & 0 & \dfrac{\bar{S}_{1212}^{0^{(\beta\gamma)}}}{\left(1 - D_I^{(\beta\gamma)}\right)} \end{bmatrix} \tag{13}$$

Initially, the crack band is free of any shear tractions. To prevent numerical instabilities, the crack band orientation is fixed for a particular subcell, upon initiation. Thus, the $\bar{S}_{1313}^{(\beta\gamma)}$ and $\bar{S}_{1212}^{(\beta\gamma)}$ shear compliances in

Downloaded by Evan Pineda on April 26, 2013 | http://arc.aiaa.org | DOI: 10.2514/6.2013-1474

This material is declared a work of the U.S. Government and is not subject to copyright protection in the United States.

the rotated frame are degraded, as well as the $\bar{S}_{1111}^{(\beta\gamma)}$ compliance, so that the faces of the cracks within the band normal to $\boldsymbol{n}_{\mathbf{1}}^{(\boldsymbol{\beta\gamma})}$ are free of normal and shear tractions when all of the crack band energy has been dissipated (i.e. $l_C^{(\beta\gamma)} W_F^{(\beta\gamma)} = \mathcal{G}_{IC}^{(\beta\gamma)}$). $W_F^{(\beta\gamma)}$ scales with $l_C^{(\beta\gamma)}$ in a discretized continuum. In reality W_F in Equation (2) is fixed; however $W_F^{(\beta\gamma)}$, which is smeared over the subcell volume, changes as a function of the characteristic subcell length. A mixed-mode law could be introduced to ensure that as shear tractions develop, the appropriate mode II strain energy release rate is dissipated. However, most mixed-mode theories utilize an initial mode mixity parameter to calculate the effective traction-separation law.[51,52] For a crack band initially oriented perpendicular to the maximum principal stress direction, this mode mixity parameter would be zero.

Once the compliance in the rotated frame is degraded, it is transformed back to the global frame to yield the new compliance of subcell $(\beta\gamma)$.

$$S_{ijkl}^{(\beta\gamma)} = T_{pi}^{-1} T_{qj}^{-1} \bar{S}_{pqrs}^{(\beta\gamma)} T_{kr}^{-1} T_{ls}^{-1} \tag{14}$$

Although only one direction is damaged in the principal frame, when transformed back to the global frame any general direction may accumulate damage. Additionally, damage introduced in the principal frame, through Equation (13), can induce normal-shear coupling in the global frame.

If the maximum principal stress is compressive, then any initiated crack band closes and the rotated compliance tensor is modified to reflect this.

$$\bar{\boldsymbol{S}}^{(\boldsymbol{\beta\gamma})} = \begin{bmatrix} \bar{S}_{1111}^{0^{(\beta\gamma)}} & \bar{S}_{1122}^{(\beta\gamma)} & \bar{S}_{1133}^{(\beta\gamma)} & 0 & 0 & 0 \\ \bar{S}_{1122}^{(\beta\gamma)} & \bar{S}_{2222}^{(\beta\gamma)} & \bar{S}_{2233}^{(\beta\gamma)} & 0 & 0 & 0 \\ \bar{S}_{1133}^{(\beta\gamma)} & \bar{S}_{2233}^{(\beta\gamma)} & \bar{S}_{3333}^{(\beta\gamma)} & 0 & 0 & 0 \\ 0 & 0 & 0 & \bar{S}_{2323}^{(\beta\gamma)} & 0 & 0 \\ 0 & 0 & 0 & 0 & \dfrac{\bar{S}_{1313}^{0^{(\beta\gamma)}}}{\left(1 - D_I^{(\beta\gamma)}\right)} & 0 \\ 0 & 0 & 0 & 0 & 0 & \dfrac{\bar{S}_{1212}^{0^{(\beta\gamma)}}}{\left(1 - D_I^{(\beta\gamma)}\right)} \end{bmatrix} \tag{15}$$

Damage can no longer evolve under compression conditions, and the stiffness in the direction perpendicular to the crack band reverts to its undamaged value. The shear stiffness in the plane of the crack band remains at the previously attained, maximum degradation state. Ref. 45,46 implemented a Mohr-Coulomb initiation criterion, and mode II evolution law, to allow shear cracks to develop under a principally compressive stress state. This formulation is omitted from this paper for brevity. The focus of this paper is to demonstrate the necessity for energy preservation across the scales. An example is chosen that ensures local, tensile stress states in the principal directions, and no prediction of compressive failure is attempted.

III. Multiscale Modeling of Composite Structures Using GMC

RUCs modeled with GMC can be easily linked to higher-level, structural FEM models. The integration point strains, from the FEM model, are applied to the RUC and the local subcell fields are determined using GMC; this process is referred to herein as down-scaling for clarity, although in literature it is more often referred to as localization. If the subcell material behavior is nonlinear, the local stresses and strains are used to calculate the local stiffnesses, inelastic strains, thermal strains, and/or state variables. Since the local stresses and strains depend on the local stiffnesses, inelastic strains, and thermal strains, some iterations of this procedure may be necessary to resolve the correct local fields if there is a high degree of nonlinearity. The RUC is then homogenized and the global stiffnesses, inelastic strains, thermal strains, and/or state variables are computed and passed onto the macroscale in a process referred to as up-scaling.

Downloaded by Evan Pineda on April 26, 2013 | http://arc.aiaa.org | DOI: 10.2514/6.2013-1474

This material is declared a work of the U.S. Government and is not subject to copyright protection in the United States.

The global stresses and material Jacobian at the integration point are then computed using the up-scaled, global, homogenized fields. A schematic showing this procedure and the corresponding scales is presented in Figure 4.

Since failure is dictated by extreme values, it is hypothesized that the fiber-matrix architecture influences the evolution of failure, as it influences the local extreme values. The extreme values are a result of non-homogeneity due to property mismatch between constituents, and geometrical packing details of the constituents. Therefore, failure is modeled at the microscale, within GMC, using the crack band approach presented in Section II. Homogenization of the microscale is used to influence failure mechanisms at the higher scales (in this two-scale case, the higher scale being macroscale).

III.A. Preserving Energy Across Scales Using Consistent 'Handshaking' Methods

In order to retain mesh objectivity in a multiscale model, both the energy density and energy release rate must be preserved at, and across, all scales. Utilizing the crack band model (see Section II) within the GMC micromechanics ensures objectivity at the microscale. However, there must be a consistent relationship between the characteristic lengths at each scale in order to preserve the energy release rate.

Communication between the finite element integration points and the GMC RUC is achieved through the global stress $\bar{\boldsymbol{\sigma}}$ and strain $\bar{\boldsymbol{\epsilon}}$ measures, see Figure 5. The global stress and strains are the fields at corresponding element integration points and also represent the average global stresses and strains applied to the RUC. In addition the material Jacobian, or tangent stiffness matrix, of the RUC calculated by GMC can be passed to the FEM and used to formulate the element stiffness matrix and/or estimate the next global strain increment.

The energy density can be defined at the microscale for the RUC

$$W^{RUC} = \int \bar{\sigma}_{ij}^{RUC} d\bar{\epsilon}_{ij}^{RUC} \tag{16}$$

where $\bar{\sigma}_{ij}^{RUC}$ and $\bar{\epsilon}_{ij}^{RUC}$ are the components of the global, average stress and strain tensors applied to the RUC, and the energy density can be defined at the macroscale for an integration point

$$W^{int} = \int \bar{\sigma}_{ij}^{int} d\bar{\epsilon}_{ij}^{int} \tag{17}$$

where $\bar{\sigma}_{ij}^{int}$ and $\bar{\epsilon}_{ij}^{int}$ are the components of the stress and strain tensors at the finite element integration point.

Since, using the previously described handshaking method, the global stresses and strains are maintained across the scales (i.e., $\bar{\sigma}_{ij}^{int} = \bar{\sigma}_{ij}^{RUC}$ and $\bar{\epsilon}_{ij}^{int} = \bar{\epsilon}_{ij}^{RUC}$, it follows that the energy density is automatically preserved.

$$W^{int} = W^{RUC} \tag{18}$$

The energy density for the finite element can be taken as the volume averaged sum of the energy density of all the integration points within that finite element

$$W^{e} = \frac{1}{V^{e}} \sum_{int=1}^{nint} W^{int} V^{int} \tag{19}$$

where V^{int} and V^{e} are the integration point subvolumes and element volume, respectively.

In addition to the energy density, the energy release rate must be preserved across the scales. The energy release rate, or fracture energy, is defined as the energy density (in the absence of plastic strain accumulation) multiplied by some characteristic length associated with the localization band.[36, 39, 53–55] Thus, the total energy release rate for the RUC at the microscale is given by

$$\mathcal{G}^{RUC} = l_C^{RUC} W^{RUC} \tag{20}$$

where l_C^{RUC} is the charateristic material length associated with strain softening in the RUC. Similarly, the energy release rate for the integration point at the macroscale is defined as

$$\mathcal{G}^{int} = l_C^{int} W^{int} \tag{21}$$

Downloaded by Evan Pineda on April 26, 2013 | http://arc.aiaa.org | DOI: 10.2514/6.2013-1474

This material is declared a work of the U.S. Government and is not subject to copyright protection in the United States.

where l_C^{int} is the characteristic length associated with the integration point. It follows that the total energy release rate of the finite element is obtained from the volume averaged sum of the energy release rates of the integration points.

$$\mathcal{G}^e = \frac{1}{V^e} \sum_{int=1}^{nint} \mathcal{G}^{int} V^{int} \tag{22}$$

In order for the energy release rates at both scales to be equal, the characteristic lengths associated with the finite element integration point and the RUC must equivalent. At the subcell level, it is trivial to define the characteristic length, $l_C^{(\beta\gamma)}$ (see Section II.A)—it is simply the length of the subcell perpendicular to the crack band. However, the characteristic length of the RUC is a result of the evolution of the crack band(s) in multiple subcells contained within the RUC. Since, the crack band path is complex, and the final configuration is not known *a priori* it cannot be calculated and delivered to the macroscale to ensure that the lengths are equal.

Moreover, there is a restriction placed on the minimum allowable size of the macroscale element. The element (or integration point subvolumes) must be large enough to contain the characteristic length of the RUC, or a suitably large RVE containing enough fibers needed to represent the localization objectively.[8,9,46] If the element is too small, then microscale homogenization techniques are not valid and physics is violated.

It is hypothesized here that if the size and shape of the RUC and integration point subvolume are identical, then all lengths must be consistent across the scales, automatically. This statement holds true for the characteristic lengths also, even if they cannot be calculated or defined. Unfortunately, GMC only admits rectangular RUCs (although a new isoparametric mapping technique has been developed for HFGMC[56]), and it is impractical to assume the finite element mesh will contain only rectangular elements. Particularly when modeling structural components, generally shaped quadrilaterals for 2D, or hexahedra for 3D, structures are more appropriate .

It can be assumed that the characteristic length of a 2D element integration point is equal to the square root of its area.

$$l_C^{int} = \sqrt{A^{int}} \tag{23}$$

A similar relationship can be assumed for the doubly-periodic RUC

$$l_C^{RUC} = \sqrt{A^{RUC}} \tag{24}$$

where H and L are the RUC dimensions given in Figure 3. If the dimensions H and L are scaled such that the new values (denoted by a prime symbol) are given by

$$H' = \frac{l_C^{int} H}{\sqrt{HL}} \tag{25}$$

$$L' = \frac{l_C^{int} L}{\sqrt{HL}} \tag{26}$$

then utilizing Equations (25) and (26) in Equation (24) results in equivalent characteristic lengths at both scales, that is,

$$l_C^{RUC} = l_C^{int} \tag{27}$$

Finally, substituting Equations (18) and (27) into Equations (20) and (21) yields

$$\mathcal{G}^{int} = \mathcal{G}^{RUC} \tag{28}$$

which, along with Equation (18), is a necessary condition for mesh objective multiscale modeling of strain softening behavior.

III.B. FEAMAC Multiscale Framework

In Section IV, a multiscale framework is utilized to perform simulations of fiber-reinforced composite structures by modeling the fiber-matrix architecture as an RUC at the microscale using GMC and linking the microscale to the lamina/laminate level (macrsocale) FEM model. A synergistic approach is employed that executes concurrent multiscaling in time, but two-way hierarchical multiscale in space.[11] The commercial

Downloaded by Evan Pineda on April 26, 2013 | http://arc.aiaa.org | DOI: 10.2514/6.2013-1474

This material is declared a work of the U.S. Government and is not subject to copyright protection in the United States.

Downloaded by Evan Pineda on April 26, 2013 | http://arc.aiaa.org | DOI: 10.2514/6.2013-1474

finite element software, Abaqus 6.11-1[57] is used as the FEM platform, and the MAC/GMC core micromechanics software[58, 59] is used to perform microscale calculations, and the scales are linked using the FEAMAC software implementation.[27] The number of subcells and constituents within an RUC at the microscale is completely general and as many, or as few, may be used as needed to accurately characterize the micro-architecture of the composite. Moreover, any constitutive model can be used in the subcells of the RUC to represent the mechanical or thermal response of the constituents.

FEAMAC consists of four Abaqus/Standard user defined subroutines,[57] as well as six subroutines exclusive to the FEAMAC package (see Figure 6). The Abaqus/Standard user material `UMAT` subroutine provides the strains, strain increments, and current values of state variables to MAC/GMC through the front end subroutine `FEAMAC`. For this work, crack band calculations are performed within MAC/GMC, and `FEAMAC` is called iteratively until convergence is acheived at the microscale. MAC/GMC then returns a new stiffness and stress state, as well as updated state variables, to the `UMAT` via the `FEAMAC` subroutine. The Abaqus/Standard user subroutine `SDVINI` initializes the state variables used in `UMAT`. The Abaqus/Standard user subroutine `UEXPAN` is used for thermal analysis by providing the integration point temperature, temperature increment, and current state to MAC/GMC, which in turn, calculates new thermal strains and thermal strain rates. Problem set-up task, initialization, and writing MAC/GMC level output data to files is achieved through the Abaqus/Standard user subroutine `UEXTERNALDB`, which evokes communication among Abaqus/Standard and the `FEAMAC_PRE` and `FEAMAC_PLOTS` subroutines. The reader is referred to Ref. 27 for further details on the FEAMAC software implementation. Furthermore, a wrapper (FEAMAC/Explicit) was developed to link FEAMAC to the Abaqus/Explicit FEM software through a `VUMAT` Abaqus user material subroutine.[60]

IV. Numerical Examples

IV.A. Example 1 - Finite-notched DCB

IV.A.1. Multsicale Model Details

To demonstrate the effects of appropriate microscale RUC length scaling, a simple multiscale example was chosen representing a modified DCB specimen. The global geometry of the modified DCB is shown in Figure 7. The total specimen length was 100 mm, with a height of 6 mm. Plane strain conditions were assumed. A 25.5 mm notch was placed at one end of the specimen. Since continuum elements were used to model the domain and incorporate damage, a notch with a tip of a finite diameter (1 mm) was chosen so that a converged stress solution could be obtained. If a sharp crack had been chosen, the stress concentration at the notch tip could not be calculated properly. The focus of this work was to isolate mesh dependence due to post-peak strain softening. Hence, it was desirable to eliminate the dependence of the elastic solution on the global mesh size, altogether.

The entire domain was meshed using 2D, plane strain, reduced integration, quadrilateral CPE4R, and triangular CPE3 Abaqus elements.[57] A mesh sensitivity study was conducted and it was determined that using an element size l^e (see Figure 7) of 0.075 mm, or smaller, ahead of the notch tip would yield a converged, elastic, stress state at the notch tip. Figure 8 shows the coarsest mesh used in the studies incorporating a 0.075 mm by 0.075 mm elements ahead of the notch tip. Figure 8b shows a magnified view of the mesh surrounding the notch tip. Assuming a fiber diameter of 5μm, an element of this size would contain nearly 170 fibers, which is adequate to justify the use of periodic boundary conditions, initially.

The macroscale domain lies in an x-y-z coordinate system. The model is intended to simulate matrix cracking in a 90°, IM7-8552 laminate, so the fiber direction is aligned with the global z-axis. For simplicity, and efficiency, the majority of the elements, represented with green in Figures 7 and 8, utilized a single-scale, elastic, transversely isotropic constitutive law. The elastic properties for IM7/8552 are given in Table 1.[43]

The elements along the expected macroscale crack path, represented in yellow, were linked to a microscale, GMC RUC using FEAMAC. The microscale model consisted of a 7 subcell by 7 subcell RUC with a local x_1-x_2-x_3 coordinate system. The RUC was composed of 13 subcells comprised of the fiber constituent (colored blue, see Figure 7) and 36 subcells comprised of the matrix constituent (colored green). A fiber volume fraction V_f of 60% was maintained. The axial, fiber direction, x_1, is aligned with the global z-axis. This choice of RUC may not be completely suitable once localization occurs, since the size of the localization typically spans one, or multiple, unit cells. An RVE containing multiple fibers is more appropriate to capture the effects of the microscale localization objectively. The intention of this work was not to offer blind failure predictions using the multiscale methodology, or to investigate solutions objectivity relative to

This material is declared a work of the U.S. Government and is not subject to copyright protection in the United States.

RVE size and complexity, but rather to demonstrate the necessity for energy preservation and consistent handshaking methods across the scales. Thus, the simple and efficient RUC was chosen for its computational speed advantages and tractability, so that numerous multiscale simulations could be achieved in a reasonable amount of time. Furthermore, determining an adequate size and level of detail for the RVE, when there is localization at the subscale, remains an ongoing research area.[8, 9, 46]

The elastic properties of the fiber (transversely isotropic) and matrix (isotropic) are given in Table 2. These properties were calibrated such that the global RUC properties calculated using the 7 x 7 GMC RUC corresponded to the elastic properties given in Table 1. The transverse fiber stiffness E_{22}^f, and axial shear modulus G_{12}^f were taken from Ref. 61.

The crack band theory, detailed in Section II.A, was used to dictate failure in the matrix subcells. The transverse strength and mode I fracture toughness of a unidirectional, IM7/8552 ply was reported by Ref. 43 as 62.3 MPa and 0.2774 kJ/m^2. The same, single-fiber, 7 x 7 RUC was used, assuming a fiber diameter of 5 μm, to calibrate the matrix strength and fracture toughness. Using the standalone MAC/GMC micromechanics software, The RUC was loaded under transverse strain and the matrix properties were adjusted until the global RUC exhibited a strength and total energy release rate upon failure corresponded to the values reported in Ref. 43. The resulting properties are presented in Table 3, and the stress strain response of the RUC is plotted in Figure 9. Note that the incredibly high strain to failure (> 1.5) is a result of the crack band opening displacement smeared over the subcell, not elastic strain in the material (continuum). Since the single fiber RUC utilized realistic fiber dimensions, a reasonable opening displacement yields a seemingly very large homogenized strain. At larger, structural scales, the same crack band opening displacement would produce more reasonable homogenized strains.

The focus of this work was to determine the effects of incorporating a consistent length across the scales in a multiscale analysis. The yellow domain containing multiscale elements, shown in Figures 7 and 8, utilized fixed element shapes and sizes. Since single integration point elements were used, the characteristic length of the elements and integration point subvolumes are identical.

$$l_C^e = l_C^{int} \tag{29}$$

The element sizes in front of the notch tip corresponding to the multiscale elements were decreased from 0.075 mm, the maximum allowable element size needed to obtain a converged stress state at the notch tip. Two types of analyses were performed: scaled and unscaled. Scaled analyses utilized Equations (25) and (26) to scale the dimensions of the RUC so that they corresponded to the element dimensions. Unscaled analysis assumed fixed RUC dimensions equal to 0.075 mm x 0.075 mm. When the RUC dimensions are scaled the volume of the RUC represents a physical volume, similar to an RVE. However, due to the simplicity of the fiber/matrix architecture it cannot statistically represent the heterogeneous nature of the composite and periodic boundary conditions are still utilized; thus, this scaled unit cell will still be referred to as an RUC.

In addition to two types of analyses, two types of elements were used along the notch tip front. Square elements were used as a baseline because the assumed characteristic length l_C^e (Equation (23)) and the dimensions of the element sides l^e (see Figure 7) are equivalent. Therefore, if RUC length scaling is performed, the dimensions of the RUC and the element are equal. Thus, every length definition is maintained across the scales and Equation (27) automatically holds without needing to make the assumption in Equation (23). With a consistent size and shape at both scales, the characteristic lengths do not need to be defined explicitly, yet it can be accepted that the appropriate localization limiter will be delivered to the macroscale (due to the equivalence of all length definitions) and Equation (28) will be satisfied assuredly.

In addition to square elements, triangular elements are used (see Figure 8c) wherein $l_C^e \neq l^e$. Therefore, the exact size and shape were not preserved across the scales, only the volume. Hence, not all length definitions are inherently preserved. The results from these scaled simulations will indicate if the assumption made with Equation (23) is always valid.

IV.A.2. Numerical Results

Figure 10 shows the ultimate load predicted from the two different analysis types (scaled and unscaled) utilizing two different element shapes (square and triangular). The element size was varied from 0.075 mm to 0.045 mm (which could still accommodate 61 fibers at a 60% fiber volume fraction) in increments of 0.05 mm. Results from analyses using square element are indicated with square symbols, and results from analyses using triangular elements are indicated with triangular symbols. Filled markers signify that the

Downloaded by Evan Pineda on April 26, 2013 | http://arc.aiaa.org | DOI: 10.2514/6.2013-1474

This material is declared a work of the U.S. Government and is not subject to copyright protection in the United States.

RUC dimensions were scaled according to the assumed characteristic element length (Equation (23)) using Equations (25) and (26), and open markers denote that a fixed RUC size of 0.075mm x 0.075mm was used.

When square elements with scaled RUCs were used, the ultimate load predicted during the simulations remained within 1% of the mean 8.02 N. Whereas, not performing the scaling appropriately led to a steady reduction in the ultimate load as the element size was decreased. Using a square element with length 0.045 mm, and an unscaled RUC, yielded an ultimate load prediction of 7.02 N, a 13.5% error from the mean of the scaled analyses. This pathological mesh dependence is the most significant limitation of multiscale modeling identified by Ref. 50, as it yields inconsistent and unreliable predictions. However, as shown, with the appropriate "handshaking" methodology and the use mesh independent damage theories at the microscale, this pathological dependence on the discretization size can be altogether eliminated at all scales.

Scaling also eliminates pathological mesh dependence when using triangular elements as shown in Figure 10. The ultimate load predictions vary from the mean by 1%, at most. However, the mean ultimate load obtained from the simulations utilizing triangular elements varies from the mean ultimate load results calculated using square elements by 9.4%. This significant error indicates that the estimate of the characteristic length using Equation (23) is incorrect for triangular elements. When the scaling is not implemented, the ultimate load prediction pathologically decreased as the size of the triangular elements was reduced resulting in a maximum error from the mean of 21% with an element size of 0.045 mm.

It should be noted that in Figure 10, unscaled results obtained using both element types are comparable. Since a fixed RUC size is used, the effects of the scaling are eliminated from the problem, and the displayed trends are purely a result of the change in the element size. This indicates that a better estimate of the localization limiter may have been the width of the advancing macroscale softening band (localization),

$$l_C^e = l^e \tag{30}$$

not the assumed characteristic element length computed using Equations (23) and (29).

The ultimate load predictions obtained when the RUC dimensions are scaled according to Equation (30) are displayed in Figure 11 along with the previous results obtained from the scaled simulations (utilizing both square and triangular elements). The lines represent the mean value for the corresponding simulations. It can be observed that using the element length rather than the square root of the area of the element improves the results for the simulations utilizing triangular elements. The mean error using square elements improved from 9.4% to 1%; however the results are not identical.

For the problem demonstrated, where the macroscale localization growth is self-similar, it may seem that a suitable localization limiter would be the width of the macroscale localization band. However, if the crack band path at the microscale is not known beforehand it is impossible to assume the localization limiter at the macroscale because it is inherently coupled to the localization length(s) at the microscale.

IV.B. Example 2 - 2D Plane Strain Square Section

IV.B.1. Multsicale Model Details

A second example, first presented in Ref. 62, is included in this manuscript to further demonstrate the necessity for appropriate "handshaking" in order to yield a mesh objective and energetically accurate solution. In this multiscale example, the macroscale was composed of a square domain meshed using plane strain quadrilateral elements (see Figure 12) or plane strain triangular elements (see Figure 13). As in the previous example, square elements are used to establish a baseline solution wherein size *and* shape of the finite elements and microscale RUCs are identical; thus, preserving all other possible definitions of length across the scales.

Failure is introduced into the matrix subcells of the microscale RUC, and the effects are transferred to the macroscale through an overall reduction of the stiffness of the RUC (due to a local reduction in the stiffness of the failing matrix subcells). The crack band model presented in Section II is used to govern failure at the microscale. Only the yellow and red elements in Figures 12 and 13 were modeled with multiscale FEAMAC elements. The green elements were modeled using the Abaqus elastic material model. Free edge effects and the accuracy of the local fields surrounding the failure path front are influenced by the mesh refinement, to some degree, which may affect the failure path in the simulation. Therefore, failure was restricted to the yellow and red elements to simplify the problem as much as possible and try to ensure that the energy dissipated in the model is a result of the multiscale methodology, not other influences. Moreover, the matrix subcells of the RUC located in the red element were given a slightly lower cohesive strength than the matrix

Downloaded by Evan Pineda on April 26, 2013 | http://arc.aiaa.org | DOI: 10.2514/6.2013-1474

This material is declared a work of the U.S. Government and is not subject to copyright protection in the United States.

of the RUCs within the yellow elements. This was imposed to imitate an imperfection and facilitate the localization of initial failure into a single element. Without this imperfection, all of the FEAMAC elements would fail simultaneously because the stress and strain fields are uniform throughout the FEM mesh. After failure initiates in the RUC located in the red element, failure progresses into the RUCs located within the adjacent yellow elements until the failure reaches the free edge of the FEM mesh.

The microscale RUCs are linked to the macroscale integration points such that the global (macro) z- and local (micro) x_1-axes are aligned. Thus, the fibers can be considered running "out of the page." The local, transverse, x_2-direction is coincident with the global x-direction, as is the the local x_3 with the global y.

Reduced integration elements were used in both the square and triangular element cases. Therefore, Equation (29) holds. Furthermore, the definition of characteristic length defined by Ref. 57 is utilized (Equation (23)). Two types of multiscale simulations were performed: scaled and unscaled. For the scaled analysis the dimensions of the RUC were scaled according to Equation (27), assuming Equation (24). Unscaled simulations incorporated a fixed length for the sides of the RUC equal to 5.98 μm.

Several simulations were performed with various levels of macroscale mesh refinement. In all simulations, the left edge of the macrsocale domain was fixed in the x-direction, while the bottom edge was fixed in the y-direction, and a uniform displacement was applied to the right edge in the x-direction. The domains were loaded until final failure; i.e., a complete loss in load carrying capability.

IV.B.2. Numerical Results

Figure 14 shows the strain energy release rate ($\mathcal{G}$) as a function of macroscale characteristic element length at final failure for the numerous different simulations. Simulations performed using square elements are shown with square data points, while triangular elements are indicated with triangular symbols. Filled symbols denote that a scaled analysis was performed, while unfilled symbols mark unscaled analyses.

The element length that is closest to the realistic size of the RUC (L = 5.98 μm) is an element length of 5.99 μm (167 elements x 167 elements), and is only 0.17% larger than the actual RUC length. Thus, the scaled solution obtained with = 5.99 μm is considered to be the most accurate solution. For this mesh, $\mathcal{G}$ was calculated to be 0.227 kJ/m2; this value will be used as the baseline energy release rate for comparison with the other simulations. The most erroneous $\mathcal{G}$ for the scaled simulations utilizing square elements was calculated from the solution using the coarsest mesh (32.3 μm), and was 16% higher than the baseline solution; although, the element length was 438.7% larger. As the mesh was refined, $\mathcal{G}$ approached 0.227 kJ/m2.

If the dimensions of the RUC were not scaled, the error observed in the energy release rate was very significant. The coarsest mesh using square elements exhibited 209.6% error from the baseline. Although, when the characteristic length of the integration point domain and the size of the RUC are comparable (i.e., 5.99 μm), $\mathcal{G}$ only exhibited 1.6% difference from the baseline. However, the energy release rate calculated for the unscaled simulations dropped suddenly when the element size approached the size of the RUC. For example, the average $\mathcal{G}$ for the next three largest meshes (6.14 μm, 7.41 μm, and 8.70 μm) is 44.5% higher than the baseline.

This example also demonstrates that scaling the size of the RUC such that it corresponds to the dimensions of the finite element minimizes the error. The variation that is observed in simulations with scaling, as the mesh is refined, can be attributed to local effects in the macroscopic FEM model such as an increase in the stress concentration ahead of the failure path front, as the mesh is refined.

The simulations incorporating triangular meshes exhibited an overall larger degree of error (when compared to the baseline) in the strain energy release rate. This is to be expected, since the shape the element and the shape of the RUC are disparate. The characteristic element length, calculated using Equations (23) and (29), that was closest to the assumed actual RUC length used in the unscaled simulations, is 5.94 μm. When the RUC dimensions were scaled, $\mathcal{G}$ was calculated to be 21.6% higher than the the baseline calculated using square elements. The largest $\mathcal{G}$ calculated (when RUC scaling was enforced), corresponding to the coarsest mesh with (33.7 μm), was 74.9 % higher than the baseline.

For the unscaled simulations utilizing a triangular mesh, the largest $\mathcal{G}$ calculated corresponded to the coarsest mesh (33.7 μm), and was 281% larger than the baseline. The smallest $\mathcal{G}$ calculated was 23.8%, corresponding to an elements size of 6.15 μm. The mismatch between the element shape and the RUC shape introduces some error when compared to the baseline square solution, just as with Example 1. Thus, the use of triangular elements in an FEAMAC simulation should be avoided. However, the error introduced

Downloaded by Evan Pineda on April 26, 2013 | http://arc.aiaa.org | DOI: 10.2514/6.2013-1474

This material is declared a work of the U.S. Government and is not subject to copyright protection in the United States.

through refining the mesh can be minimized by scaling the RUC dimension by the characteristic length of the element.

V. Conclusions

A mesh objective crack band theory for modeling post-peak strain softening was implemented within the GMC micromechanics theory. Use of the proposed methodology is shown to lead to mesh objectivity in the macroscale model in a multiscale computation. In multisclae computations, there is no guarantee that mesh-objectivity at the subscale will automatically ensure mesh objectivity at the higher scales. To ensure mesh objectivity throughout, both the energy density and energy release rate must be preserved across all scales. To achieve this, some consistent, localization limiter must be delivered to the macroscale, as discussed in Ref. 50.

The multiscale method proposed here uses the FEAMAC framework to link the MAC/GMC micromechanics software (which contains implementations of GMC) to the Abaqus finite element software. In this synergistic methodology, integration point strains are passed to the microscale in the down-scaling step. Micromechanics calculations are performed, and the global RUC stiffness (material Jacobian) and stresses are passed back to the macroscale integration point in the up-scaling step. Equilibrium is ensured at each scale through iterations.

It was hypothesized that if the dimensions of the microscale RUC were scaled according to a characteristic macroscale element length, then the ensuing computational results would be insensitive to changes in the macroscale mesh. It was assumed that the characteristic element length was equal to the square root of the element area (for 2D elements). This would ensure that, if square elements were used, both the size and shape of the RUC and element would be identical. Thus, any possible length definition would be preserved across the scales.

To test this hypothesis, two simple numerical examples were devised, and two types of analyses were performed: scaled and unscaled. Scaled analyses utilized the scaling procedure described previously, in lieu of fixed RUC dimensions; whereas unscaled analyses utilized the baseline RUC dimensions. Additionally, both square and triangular elements were utilized in the simulations, separately. If the scaling was enacted, the ultimate load predictions were insensitive to refinements in the macroscale mesh. However, if the RUC dimensions were fixed, the predicted ultimate load continued to drop as the element size was decreased, displaying pathological mesh dependence. This trend was true for both the square and triangular elements, but the scaled triangular elements produced a mean ultimate load higher than the square elements. This indicates that the assumed localization limiter used to scale the RUC for the triangular elements was dependent on the localization; therefore, the width of the global localization band was used to scale the RUC in the case of triangular elements. This gave improved results. However, the macroscale and microscale localization paths are heavily coupled and typically not known prior to simulation or testing of more complex structural components. Furthermore, the choice of an RUC may not be appropriate to represent the microstructural behavior when localization occurs. Instead, a sufficiently large RVE may need to be used. Further studies must be conducted to determine the size and complexity of the RVE needed to capture microscale deformation localization objectively.

The results of this study further support the argument that a suitable localization limiter must be delivered to the macroscale.[50] However, if the size and shape of the macroscale problem correspond directly to the size and shape of the macroscale element, then the correct localization limiter is maintained even it is not defined. Unfortunately, most realistic structural components cannot be meshed using rectangular or square elements. Therefore, the challenge remains to calculate a physically justified, fully general, macroscale localization limiter to be used to scale the RUC. This is not trivial as the macroscale localization limiter depends inherently on the microscale localization path, which is not known in advance.

Downloaded by Evan Pineda on April 26, 2013 | http://arc.aiaa.org | DOI: 10.2514/6.2013-1474

This material is declared a work of the U.S. Government and is not subject to copyright protection in the United States.

Property	Value
E_{zz}	171.4 GPa
E_{xx}	9.08 GPa
ν_{zx}	0.32
G_{zx}	5.29 GPa

Table 1: Elastic transversely isotropic properties for IM7/8552 lamina used in single scale elements.[43]

8552 Matrix Properties	Value	IM7 Fiber Properties	Value
E^m (calibrated)	4.97 GPa	E_{11}^f (calibrated)	286 GPa
ν_m (calibrated)	0.36	E_{22}^f[61]	12.4 GPa
		ν_{12}^f (calibrated)	0.29
		ν_{23}^f (calibrated)	0.29
		G_{12}^f[61]	20.0 GPa

Table 2: Elastic properties of IM7 carbon fiber and 8552 epoxy matrix constituents used in microscale GMC RUC.

Mode I Cohesive Strength $\sigma_C^{(\beta\gamma)}$	Mode I Fracture Toughness $\mathcal{G}_{IC}^{(\beta\gamma)}$
56.5 MPa	0.266 kJ/m^2

Table 3: Crack band failure parameters used in 8552 matrix subcells.

Downloaded by Evan Pineda on April 26, 2013 | http://arc.aiaa.org | DOI: 10.2514/6.2013-1474

This material is declared a work of the U.S. Government and is not subject to copyright protection in the United States.

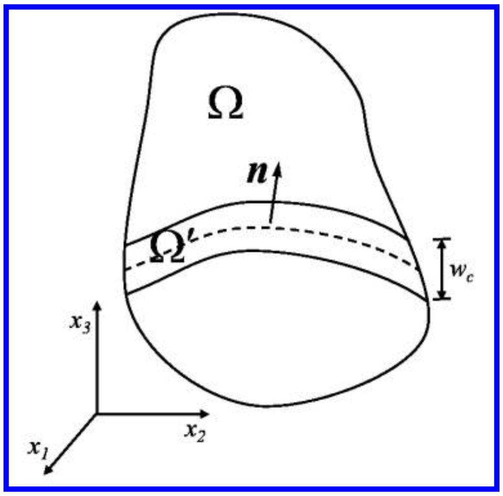

Figure 1: Crack band domain Ω' of width w_c oriented normal to vector $\boldsymbol{n}$ within a continuum Ω.

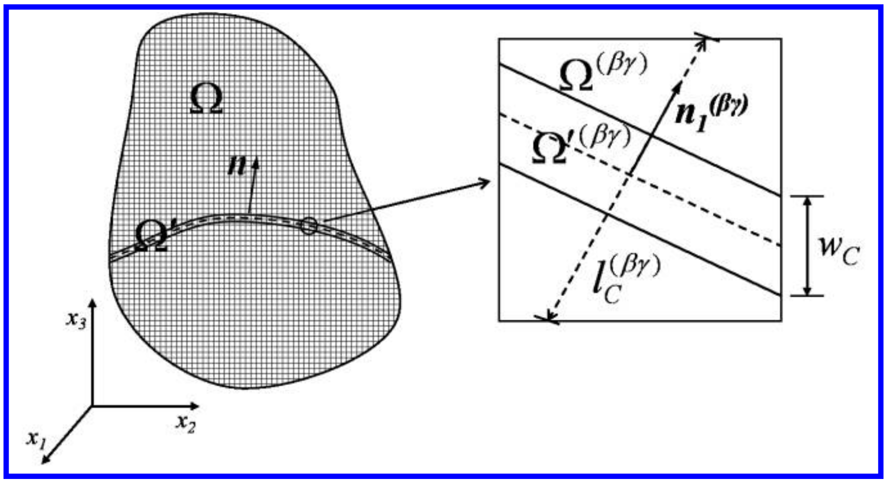

Figure 2: Crack band embedded in discretized continuum. Magnified discretization element displays crack band orientation, as well as, characteristic length of discretization element.

Downloaded by Evan Pineda on April 26, 2013 | http://arc.aiaa.org | DOI: 10.2514/6.2013-1474

This material is declared a work of the U.S. Government and is not subject to copyright protection in the United States.

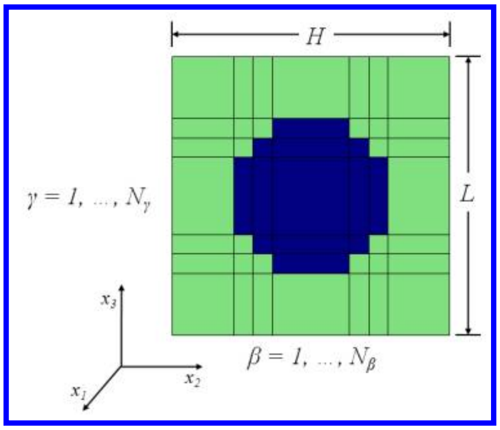

Figure 3: Doubly-periodic representation of a unidirectional, fiber-reinforced composite containing square-packed fibers using GMC.

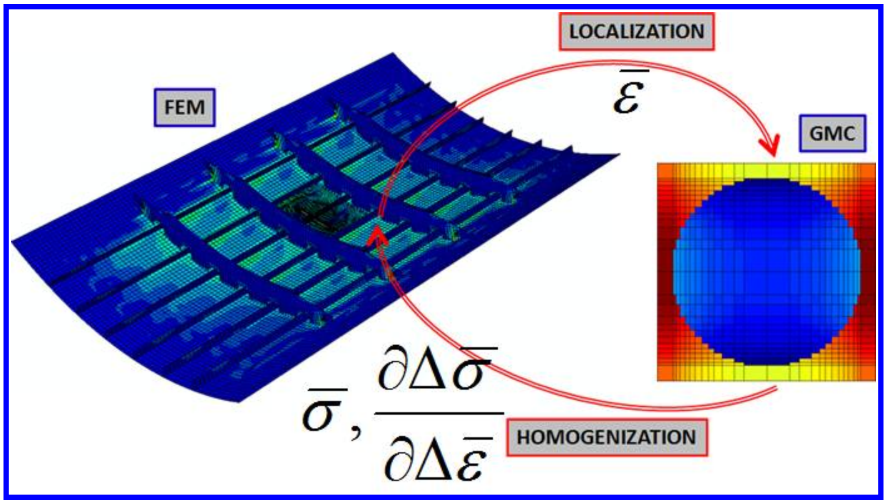

Figure 4: Schematic representation of the up-scaling and down-scaling steps employed in the synergistic multiscale technique utilizing GMC and FEM.

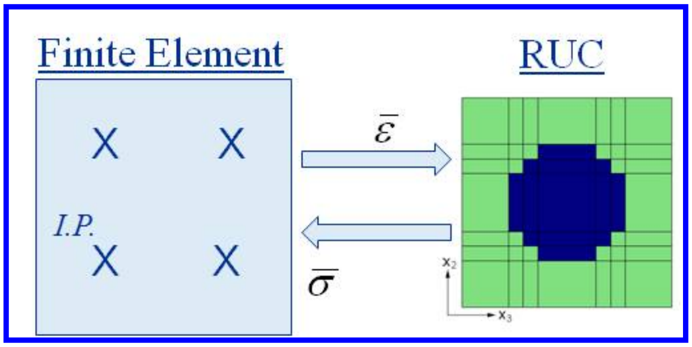

Figure 5: Schematic communication between macroscale finite element integration point and microscale GMC RUC. Global strains are passed down to the microscale and global stresses are passed back up to the macroscale.

Downloaded by Evan Pineda on April 26, 2013 | http://arc.aiaa.org | DOI: 10.2514/6.2013-1474

This material is declared a work of the U.S. Government and is not subject to copyright protection in the United States.

Downloaded by Evan Pineda on April 26, 2013 | http://arc.aiaa.org | DOI: 10.2514/6.2013-1474

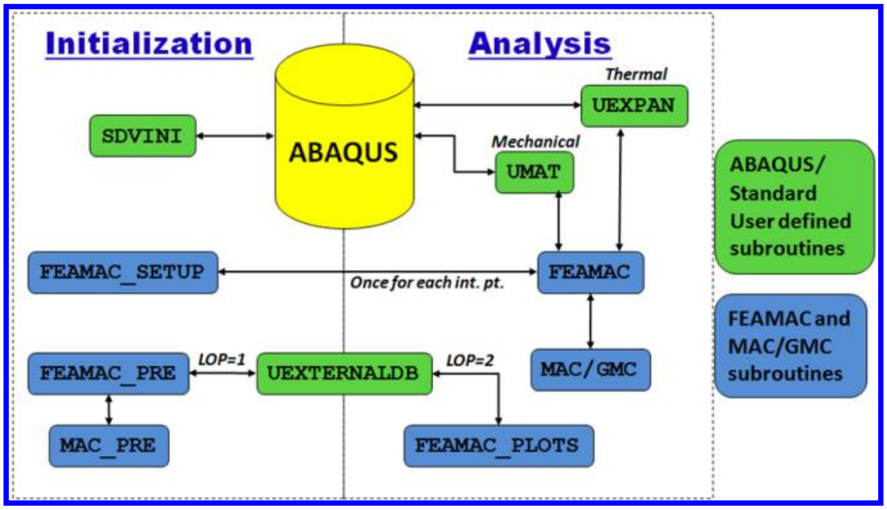

Figure 6: FEAMAC multiscale framework software implementation architecture.

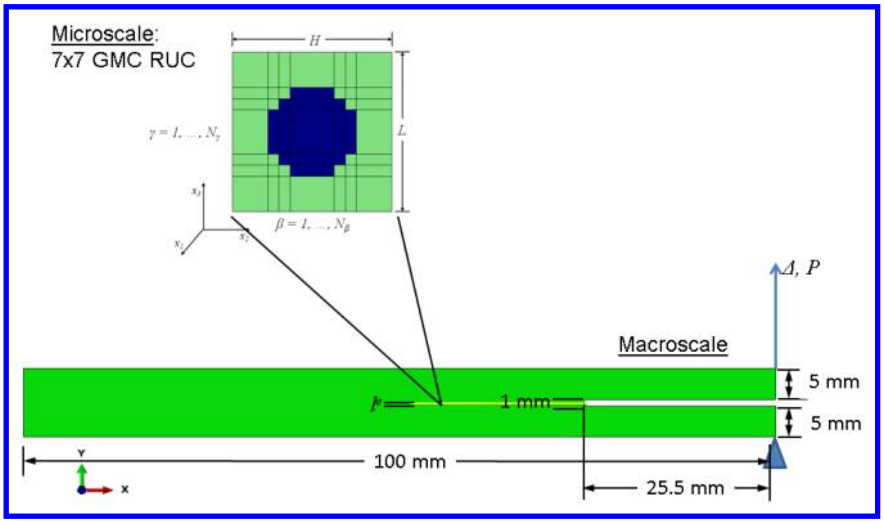

Figure 7: Multiscale model of finite-notched DCB specimen composed of a 90° laminate. The macroscale domain was modeled using traditional plane strain elements and the global x-y-z coordinate system. Elements within the green domain utilized a single-scale, transversely isotropic, constitutive law (z-axis represents the fiber direction). Elements within the yellow domain, ahead of the notch tip, were linked to a microcale GMC RUC. The microscale RUC consisted of a doubly-periodic, 7 subcell by 7 subcell RUC with a local x_1-x_2-x_3 coordinate system. The RUC contained 13 fiber subcells (colored blue) and 36 matrix subcells (colored green), and the local fiber direction, x_1, was aligned with the global z-axis.

This material is declared a work of the U.S. Government and is not subject to copyright protection in the United States.

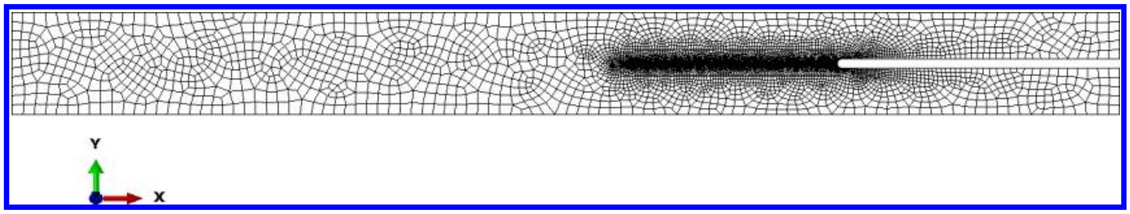

(a) Global view.

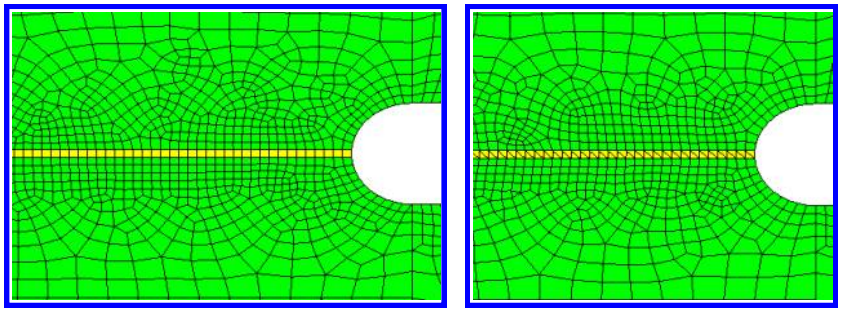

(b) Magnified view of square element mesh near notch tip.

(c) Magnified view of triangular element mesh near notch tip.

Figure 8: FEM mesh of multiscale modified DCB.

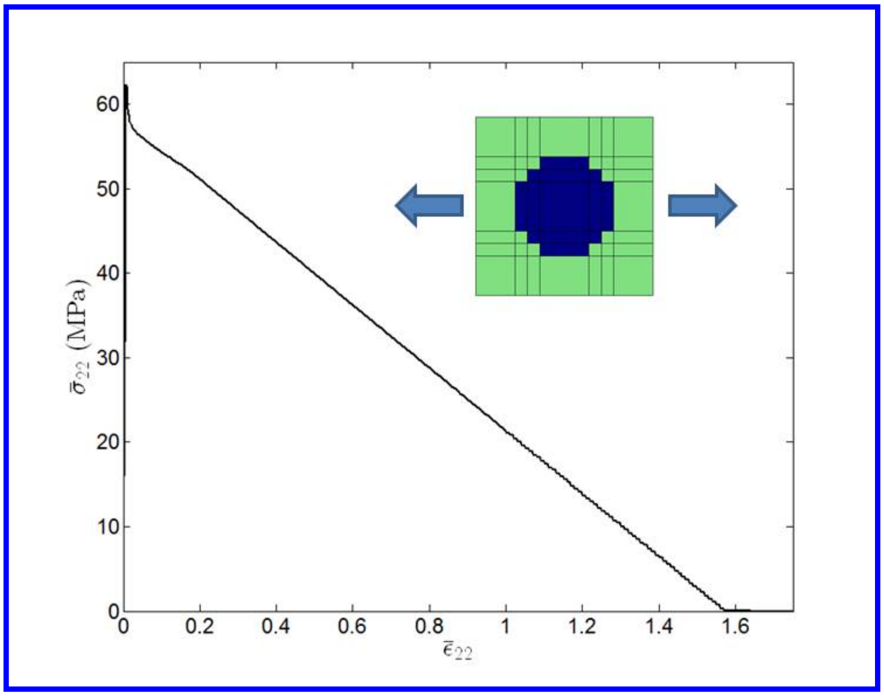

Figure 9: Global Transverse stress versus transverse strain response of RUC assuming a 5 μm diameter fiber and 60% fiber volume fraction. Matrix failure parameters were calibrated so that global RUC strength and energy release rate upon failure equaled values reported in Ref. 43 for IM7/8552.

Downloaded by Evan Pineda on April 26, 2013 | http://arc.aiaa.org | DOI: 10.2514/6.2013-1474

This material is declared a work of the U.S. Government and is not subject to copyright protection in the United States.

Downloaded by Evan Pineda on April 26, 2013 | http://arc.aiaa.org | DOI: 10.2514/6.2013-1474

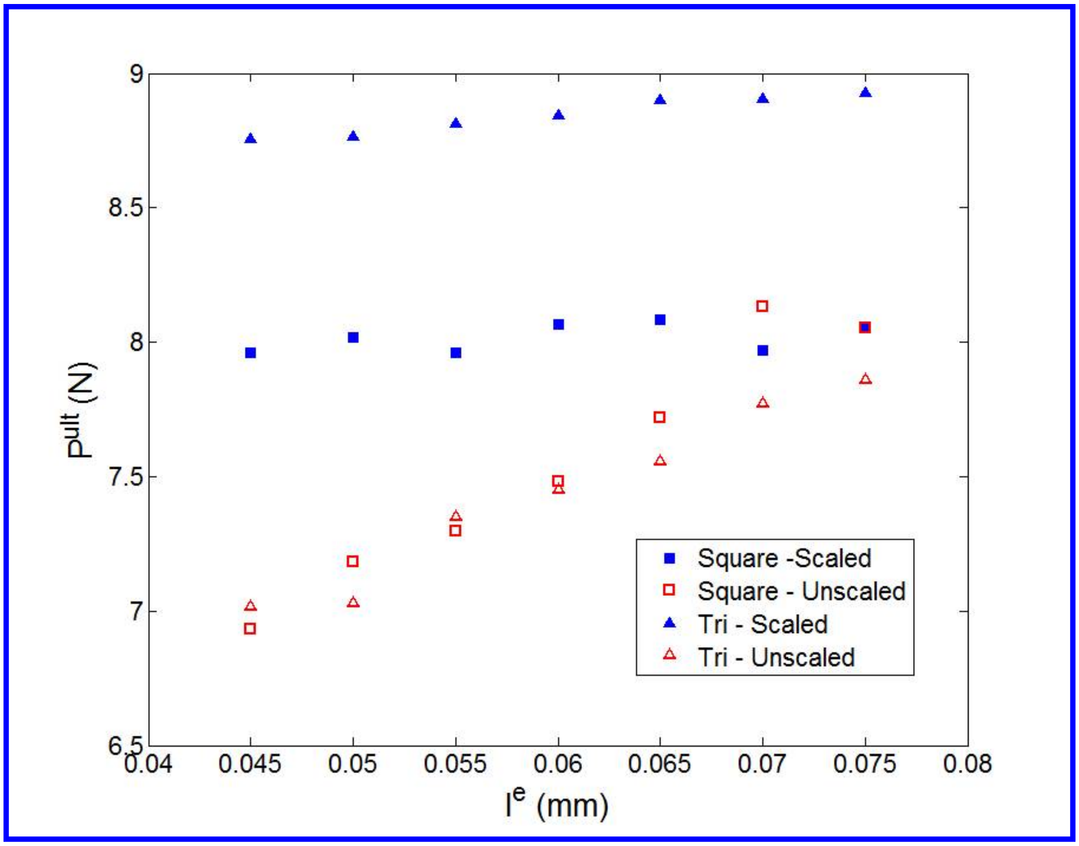

Figure 10: Ulitmate load predicted with multiscale, modified DCB simulations. Results compared for microscale RUC scaled by element length to fixed RUC dimensions of 0.075 mm x 0.075 mm. Results using square and triangular elements also compared.

This material is declared a work of the U.S. Government and is not subject to copyright protection in the United States.

Downloaded by Evan Pineda on April 26, 2013 | http://arc.aiaa.org | DOI: 10.2514/6.2013-1474

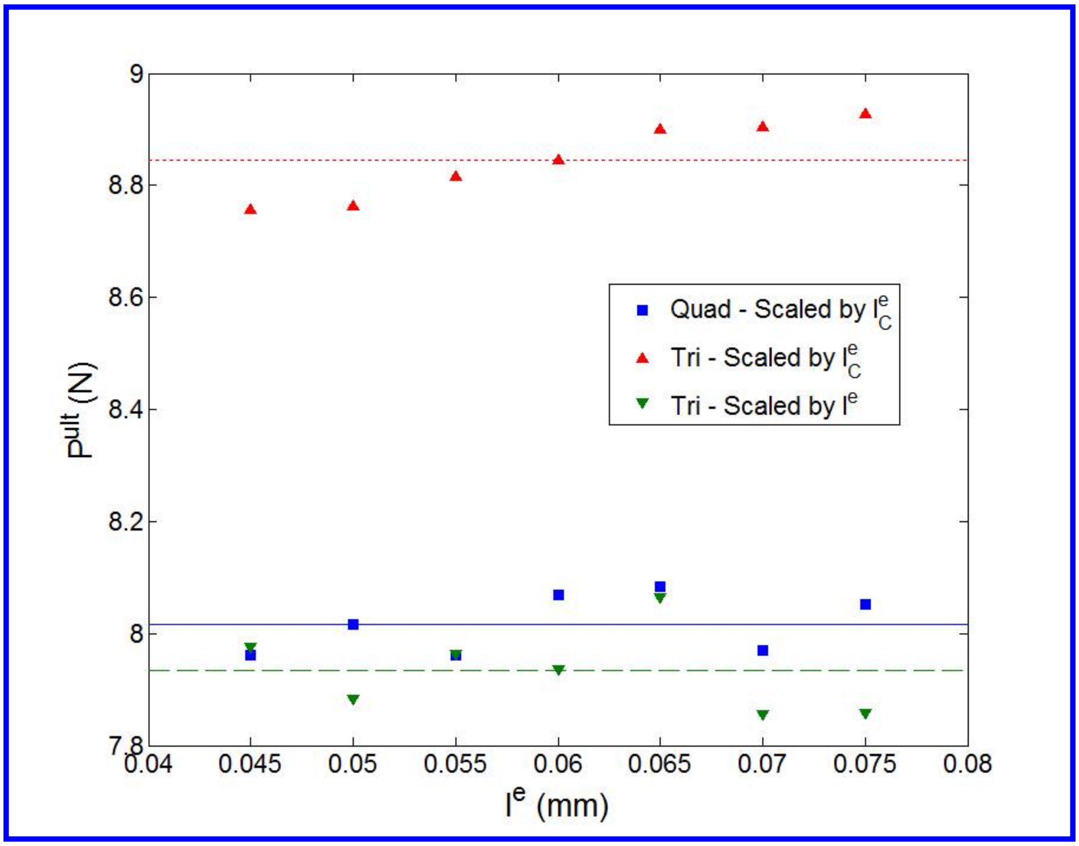

Figure 11: Ulitmate load predicted with multiscale, modified DCB simulations. Results for microscale RUC scaled by assuming two different measures for characteristic element length. Results using square (previous results, from Figure 10) and triangular elements also compared. Lines represent mean values of corresponding simulations

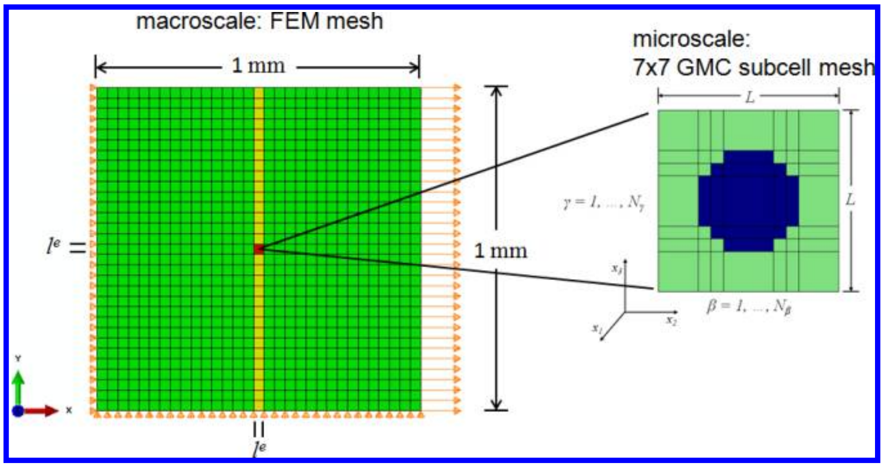

Figure 12: Multiscale example problem. Macroscale FEM model consists of square, 2-D, plane strain, reduced integration CPE4R elements with dimensions le x le and global x-y-z coordinate system. The microscale model consists of a doubly-periodic, 7 subcells x 7 subcells GMC RUC with local x1-x2-x3 coordinate system. The RUC contains 13 fiber subcells (colored blue), and 36 matrix subcells (colored green). The global dimension of the RUC are L x L, and the local subcell dimensions are h? x l?. The red and yellow FEM elements are linked to the microscale RUC. The subcells within the RUC in the red element is given a slightly lower cohesive strength than those in yellow elements. The green elements in the macroscale FEM mesh are modeled as a standard, transversely isotropic, elastic material with elastic properties equal to the homogenized elastic properties of the GMC RUC.

This material is declared a work of the U.S. Government and is not subject to copyright protection in the United States.

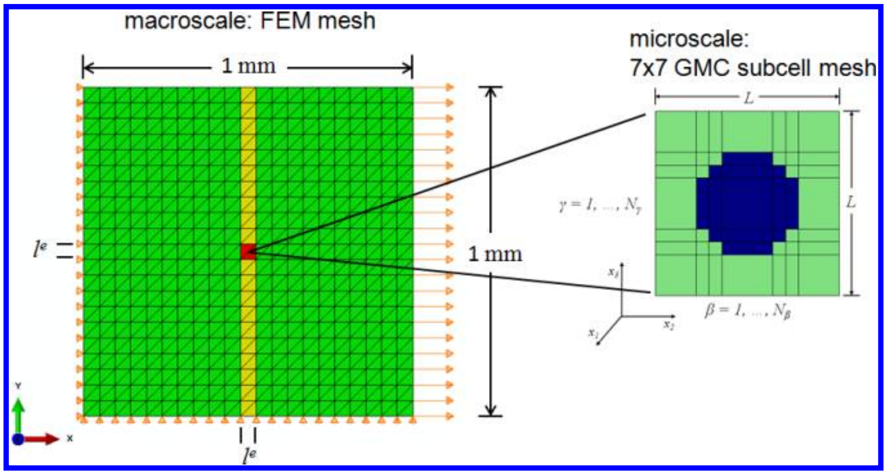

Figure 13: Multiscale simulation utilizing triangular elements at the macroscale.

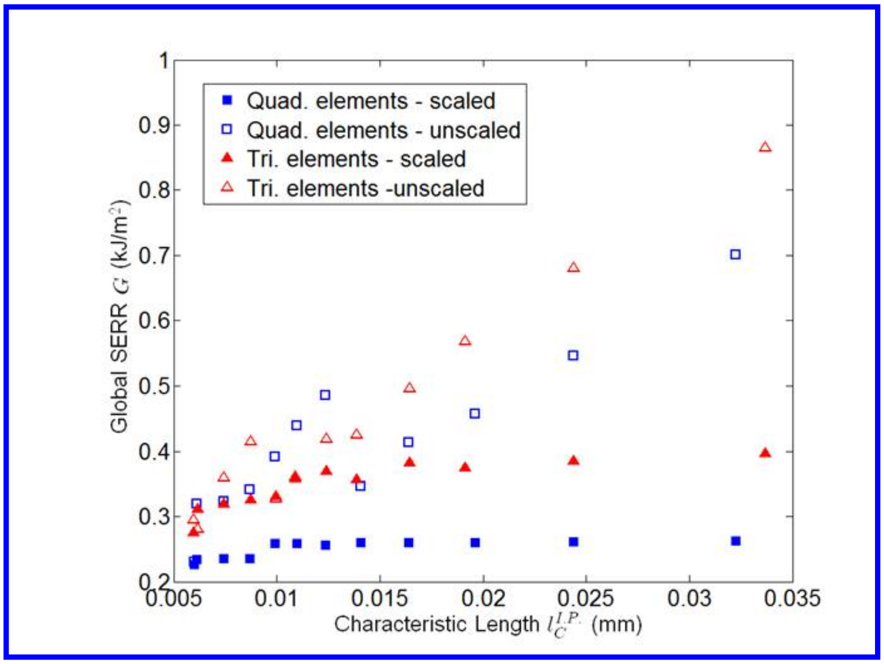

Figure 14: Total strain energy release rate (SERR) of multiscale models as a function of characteristic length.

Downloaded by Evan Pineda on April 26, 2013 | http://arc.aiaa.org | DOI: 10.2514/6.2013-1474

This material is declared a work of the U.S. Government and is not subject to copyright protection in the United States.

References

[1] Lemaitre, J. and Chaboche, J.-L., *Mechanics of Solid Materials*, Cambridge University Press, 1994.

[2] Lemaitre, J., *A Course on Damage Mechanics, 2nd Ed.*, Springer-Verlag, Berlin, Heidelberg, New York, 1996.

[3] Tay, T. E., Liu, G., Tan, V. B. C., Sun, X. S., and Pham, D. C., "Progressive failure analysis of composites," *J. Compos. Mater.*, Vol. 42, 2008, pp. 1921–1966.

[4] Tsai, S. W., *Strength and Life of Composites*, Aero & Astro, Stanford, 2009.

[5] Schuecker, C., Dávila, C. G., and Rose, C. A., "Comparison of damage models for predicting the non-linear response of laminates under matrix dominated loading conditions," NASA/TP 2010-216856, 2010.

[6] Talreja, R. and Singh, C. V., editors, *Damage and Failure of Composite Materials*, Cambridge University Press, 2012.

[7] Michel, J. C. and Suquet, P., "Non-uniform transformation field analysis: A reduced order model for multiscale non-liear problems in solid mechanics," *Multiscale Modeling in Solid Mechanics; Computational Approaches*, edited by U. Galvenetto and M. H. Aliabadi, Imperial College Press, 2010, pp. 159–206.

[8] Totry, E., Gonzaléz, C., and Llorca, J., "Influence of the loading path on the strength of fiber-reinforced composites subjected to transverse compression and shear," *Int. J. Solids Structures*, Vol. 45, 2008, pp. 1663–1675.

[9] Heinrich, C., Aldridge, M., Wineman, A. S., Kieffer, J., Waas, A. M., and Shahwan, K., "The influence of the representative volume element (RVE) size on the homogenized response of cured fiber composites," *Modelling Simul. Mater. Sci. Eng.*, Vol. 20, 2013, pp. 1–25.

[10] Prabhakar, P. and Waas, A. M., "Interaction between kinking and splitting in the compressive failure of unidrectional fiber reinforced laminated composites," *Compos. Struct.*, Vol. 98, 2013, pp. 85–92.

[11] Sullivan, R. W. and Arnold, S. M., "An annotative review of multiscale modeling and its application to scales inherent in the field of ICME," *Models, Databases, and Simulation Tools Needed for the Realization of Integrated Computational Materials Engineering: Proceedings of the Symposium Held at Materials Science & Technology 2010*, edited by S. M. Arnold and T. T. Wong, ASM International, Houston, Texas, 2011, pp. 6–23.

[12] Christensen, R. M. and Lo, K. H., "Solutions for effective shear properties in three phase sphere and cylinder models," *J. Mech. Phys. Solids*, Vol. 27, 1979, pp. 315–330.

[13] Mori, T. and Tanaka, K., "Average stresses in matrix and average energy of materials with misfitting inclusions," *Acta Metall.*, Vol. 21, 1973, pp. 571–574.

[14] Feyel, F., "Multiscale FE^2 elastoviscoplastic analysis of composite structures," *Comput. Mater. Sci.*, Vol. 16, 1999, pp. 344–354.

[15] Feyel, F. and Chaboche, J. L., "FE^2 multiscale approach for modelling the elastoviscoplastic beaviour of long fibre SiC/Ti composite materials," *Comput. Method. Appl. Mech. Eng.*, Vol. 183, 2000, pp. 309–330.

[16] Sfantos, G. and Aliabadi, M. H., "Multiscale boundary element modeling of material degradation and fracture," *Multiscale Modeling in Solid Mechanics; Computational Approaches*, edited by U. Galvenetto and M. H. Aliabadi, Imperial College Press, 2010, pp. 101–158.

[17] Suquet, P., "Elements of homogenisation for inelastic solid mechaincs," *Homogenization Techniques for Composite Media*, edited by E. Sanchez-Palencia and A. Zaoui, Vol. 272 of *Lecture Notes in Physics*, Springer, New York, 1987, pp. 193–278.

[18] Fish, J., Shek, K., Pandheeradi, M., and Shephard, M. S., "Computational plasticity for composite structures based on mathematical homogenization: Theory and practice," *Comput. Methods Appl. Eng.*, Vol. 148, 1997, pp. 53–73.

[19] Fish, J. and Yu, Q., "Multiscale damage modelling for composite materials: Theory and computational framework," *Int. J. Numer. Methods Eng.*, Vol. 52, 2001, pp. 161–191.

[20] Oskay, C. and Fish, J., "Eigendeformation-based reduced order homogenization for failure analysis of heterogeneous materials," *Comput. Methods in Appl. Mech. and Eng.*, Vol. 196, 2007, pp. 1216–1243.

[21] Ghosh, S. and Mukhopadhyay, S. N., "A two-dimensional automatic mesh generator for finite element analysis for random composites," *Comput. Struct.*, Vol. 41, No. 2, 1991, pp. 245–256.

[22] Ghosh, S., Lee, K., and Moorthy, S., "Multiscale analysis of heterogeneous elastic structures using homogenization theory and voronoi cell finite element method," *Int. J. Solids and Struct.*, Vol. 32, No. 1, 1995, pp. 27–62.

[23] Paley, M. and Aboudi, J., "Micromechanical analysis of composites by the generalized cells model," *Mechanics of Materials*, Vol. 14, 1992, pp. 127–139.

[24] Aboudi, J., "Micormechanical analysis of thermo-inelastic multiphase short-fiber composites," *Compos. Eng.*, Vol. 5, No. 7, 1995, pp. 839–850.

[25] Aboudi, J., Pindera, M.-J., and Arnold, S. M., "Linear thermoelastic higher-order theory for periodic multiphase materials," *J. Appl. Mech.*, Vol. 68, 2001, pp. 697–707.

[26] Wilt, T. E., "On the finite element implementation of the generalized method of cells micromechanics constitutive model," Nasa/cr-1995-195451, 1995.

[27] Bednarcyk, B. A. and Arnold, S. M., "A framework for performing multiscale stochastic progressive failure analysis of composite structures," *Proceedings of the 2006 ABAQUS User's Conference*, 23-25, May 2006.

[28] Pineda, E. J., Waas, A. M., Bednarcyk, B. A., and Collier, C. S., "A novel, multiscale high fidelity progressive damage and failure modeling approach for laminated fiber reinforced composites," *Proceedings of the American Society for Composites Twenty-third Technical Conference*, 7-10, Apr. 2008.

[29] Aboudi, J., Arnold, S. M., and Bednarcyk, B. A., *Micromechanics of Composite Materials: A Generalized Multiscale Analysis Approach*, Elsevier, Inc., 2013.

[30] Ladeveze, P., "Multiscale modelling and computation strategies for composites," *Int. J. Numer. Meth. Eng.*, Vol. 60, 2004, pp. 233–253.

[31] Kwon, Y. W., Allen, D. H., and Talreja, R., editors, *Multiscale Modeling and Simulation of Composite Materials and Structures*, Springer, 2008.

[32] Fish, J., editor, *Multiscale Methods: Bridging the Scales in Science and Engineering*, Oxford University Press, 2009.

Downloaded by Evan Pineda on April 26, 2013 | http://arc.aiaa.org | DOI: 10.2514/6.2013-1474

This material is declared a work of the U.S. Government and is not subject to copyright protection in the United States.

[33] Kanoute, P., Boso, D. P., Chaboche, J. L., and Schrefler, B. A., "Multiscale methods for composites: A review," *Arch. Comput. Methods Eng.*, Vol. 16, 2009, pp. 31–75.

[34] Gilat, R. and Banks-Sills, L., editors, *Advances in Mathematical Modeling and Experimental Methods for Materials and Structures: The Jacob Aboudi Volume*, Vol. 168 of *Solid Mechanics and Its Applications*, Springer, 2010.

[35] Galvenetto, U. and Aliabadi, M. H., editors, *Multiscale Modeling in Solid Mechanics; Computational Approaches*, Imperial College Press, 2010.

[36] Bažant, Z. P. and Cedolin, L., *Stability of Structures: Elastic, Inelastic, Fracture and Damage Theories*, Oxford University Press, New York, Oxford, 1991.

[37] Bažant, Z. and Cedolin, L., "Blunt crack band propagation in finite element analysis," *J. Eng. Mech. Div.-ASCE*, Vol. 105, 1979, pp. 297–315.

[38] Pietruszczak, S. and Mroz, Z., "Finite element analysis of deformation of strain-softening materials," *Int. J. Numer. Methods Eng.*, Vol. 17, 1981, pp. 327–334.

[39] Bažant, Z. P. and Oh, B. H., "Crack band theory for fracture of concrete," *Mater. and Struct.*, Vol. 16, 1983, pp. 155–77.

[40] de Borst, R. and Nauta, P., "Non-orthogonal cracks in a smeared finite element model," *Eng. Comput.*, Vol. 2, 1985, pp. 35–46.

[41] Rots, J. G. and de Borst, R., "Analysis of mixed-mode fracture in concrete," *J. Eng. Mech.*, Vol. 113, No. 11, 1987, pp. 1739–1758.

[42] Spencer, B. W., *Finite Elements with Embedded Discontinuities for Modeling Reinforced Concrete Members*, Ph.D. thesis, Brigham Young University, Provo, UT, 2002.

[43] Camanho, P. P., Maimí, P., and Dávila, C. G., "Prediction of size effects in notched laminates using continuum damage mechanics," *Compos. Sci. and Technol.*, Vol. 67, 2007, pp. 2715–2727.

[44] Pineda, E. J. and Waas, A. M., "Modelling progressive failure of fibre reinforced laminated composites: mesh objective calculations," *Aeronaut. J.*, Vol. 116, No. 1186, 2012, pp. 1221–1246.

[45] Pineda, E. J., Bednarcyk, B. A., Waas, A. M., and Arnold, S. M., "Progressive failure of a unidirectional fiber-reinforced composite using the method of cells: Discretization objective computational results," NASA/TM 2012-217649, 2012.

[46] Pineda, E. J., Bednarcyk, B. A., Waas, A. M., and Arnold, S. M., "Progressive failure of a unidirectional fiber-reinforced composite using the method of cells: Discretization objective computational results," *Int. J. Solids Struct.*, Vol. In Press, 2013.

[47] Eringen, A. C., "A unified theory of thermomechanical materials," *Int. J. Eng. Sci.*, Vol. 4, 1966, pp. 179–202.

[48] Bažant, Z. P., "Nonlocal damage theory based on micromechanics of crack interactions," *J. Eng. Mech. - ASCE*, Vol. 120, No. 3, 1994, pp. 593–617.

[49] Jirásek, M., "Nonlocal models for damage and fracture: Comparision of approaches," *Int. J. Solids Struct.*, Vol. 35, No. 31-32, 1998.

[50] Bažant, Z. P., "Can multiscale-multiphysics methods predict softening damage and structural failure?" *Mech. Amer. Acad. Mech.*, Vol. 36, No. 5-6, 2007, pp. 5–12.

[51] Ortiz, M. and Pandolfi, A., "Finite-deformation irreversible cohesive elements for three dimensional crack-propagation analysis," *Int. J. Numer. Meth.*, Vol. 44, 1999, pp. 1267–1282.

[52] Camanho, P. P. and Dávila, C. G., "Mixed-mode decohesion finite elements for the simulation of delamination in composite materials," NASA/TM 2002-211737, 2002.

[53] Rots, J. G., Nauta, P., Kusters, G. M. A., and Blaauwendraad, J., "Smeared crack approach and fracture localization in concrete," *HERON*, Vol. 30, No. 1, 1985, pp. 1–48.

[54] Oliver, J., "A consistent characteristic length for smeared cracking models," *Int. J. Numer. Meth. Eng.*, Vol. 28, 1989, pp. 461–474.

[55] Bažant, Z. P., *Scaling of Stuctural Strength*, Elsevier, Ltd., 2nd ed., 2005.

[56] Haj-Ali, R. and Aboudi, J., "A new and general formulation of the parametric HFGMC micromechanical method for two and three-dimensional multi-phase composites," *Int. J. Solids Struct.*, Vol. 50, 2013, pp. 907–919.

[57] Dassault Systèmes Simulia Corp., *Abaqus User's Manual, Vol. 1-3, Version 6.11-1*, Dassault Systèmes Simulia Corp., Providence, RI, 2011.

[58] Bednarcyk, B. A. and Arnold, S. M., "MAC/GMC 4.0 User's Manual - Keywords Manual," NASA/TM 2002-212077/VOL2, 2002.

[59] Bednarcyk, B. A. and Arnold, S. M., "MAC/GMC 4.0 User's Manual - Example Problems Manual," NASA/TM 2002-212077/VOL3, 2002.

[60] Pineda, E. J., Waas, A. M., Bednarcyk, B. A., Arnold, S. M., and Collier, C. S., "Multiscale Failure Analysis of Laminated Composite Panels Subjected to Blast Loading Using FEAMAC/Explicit," NASA/TM 2009-215813, 2009.

[61] Goldberg, R. K. and Gilat, A., "Experimental and computational characterization of the high strain rate tensile response of polymer matrix composites," *Composite Material: Testing and Design Fourteenth Volume, ASTMSTP 1436*, edited by C. E. Bakis, ASTM International, West Conshohocken, PA, 2003.

[62] Pineda, E. J., Bednarcyk, B. A., and Arnold, S. M., "Effects of subscale size and shape on global energy dissipation in a multiscale model of a fiber-reinforced composite exhibitng post-peak strain softening using Abaqus and FEAMAC," *2012 SIMULIA Community Conference*, Providence, RI, 2012.

Downloaded by Evan Pineda on April 26, 2013 | http://arc.aiaa.org | DOI: 10.2514/6.2013-1474

This material is declared a work of the U.S. Government and is not subject to copyright protection in the United States.